

Noise-induced spectral shift measured in a double quantum dot

B. Küng,^{1,*} S. Gustavsson,¹ T. Choi,¹ I. Shorubalko,^{1,2} T. Ihn,¹ S. Schön,³ F. Hassler,⁴ G. Blatter,⁴ and K. Ensslin¹

¹*Solid State Physics Laboratory, ETH Zurich, 8093 Zurich, Switzerland*

²*Electronics/Metrology/Reliability Laboratory, EMPA, 8600 Dübendorf, Switzerland*

³*FIRST Laboratory, ETH Zurich, 8093 Zurich, Switzerland*

⁴*Theoretische Physik, ETH Zurich, 8093 Zurich, Switzerland*

(Dated: September 21, 2009)

We measure the shot noise of a quantum point-contact using a capacitively coupled InAs double quantum dot as an on-chip sensor. Our measurement signals are the (bidirectional) interdot electronic tunneling rates which are determined by means of time-resolved charge sensing. The detector frequency is set by the relative detuning of the energy levels in the two dots. For nonzero detuning, the noise in the quantum point-contact generates inelastic tunneling in the double dot and thus causes an increase in the interdot tunneling rate. Conservation of spectral weight in the dots implies that this increase must be compensated by a decrease in the rate close to zero detuning, which is quantitatively confirmed in our experiment.

PACS numbers: 73.63.Kv, 73.63.Nm, 72.70.+m, 73.23.Hk

Charge detection with on-chip sensors provides a powerful tool for investigating the electronic properties of mesoscopic circuits. By performing the detection with sufficient bandwidth, the observation of single-electron charging events in real time becomes possible, which has been used, e.g., to read out the spin of quantum dots,¹ to investigate the transport statistics of interacting electrons,^{2,3} or to measure small currents.^{3,4,5} One of the simplest detectors offering enough sensitivity to perform this kind of experiments is the quantum point-contact⁶ (QPC). However, the quantum dots (QDs) that are typically probed by QPC sensors represent highly sensitive electronic devices on their own. Charge detection therefore comes with a considerable amount of back-action of the QPC on the QD to which both photons^{7,8} and phonons^{9,10} have been shown to contribute.

One way of describing the photonic part of the back-action is in terms of the shot noise of the QPC which couples capacitively to the QD system and generates photon-assisted tunneling¹¹ (PAT). From this viewpoint, the QD system can serve as a *measurement* device for the QPC noise.^{12,5} Since it works on chip, it is inherently fast, and when using a double quantum dot (DQD), frequency-tunable noise detection becomes possible via control of the interdot level detuning. In the work presented here, we use such a DQD detector to measure noise of a QPC. Owing to the sample design, with the QPC located in a different host crystal (GaAs/AlGaAs) than the noise probe (an InAs DQD), our setup features a suppression of the phononic part of the QPC-DQD interaction while maintaining an extraordinarily large capacitive coupling: QPC conductance changes caused by dot charging can exceed 50%, while the corresponding figure for split-gate or AFM-defined samples is typically a few percent.^{13,14} In contrast to previous experiments, we are able to measure the response of the DQD along the whole detuning axis from positive to negative values. In particular, we observe the reduction in the DQD tunneling rate around zero detuning in response to the QPC noise,¹¹ an effect

which is associated with the normalization of the spectral density of the dot wave functions.

Figure 1(a) shows a scanning electron microscope (SEM) image of the sample. It is fabricated by depositing an InAs nanowire on top of a GaAs/AlGaAs heterostructure containing a 37-nm-deep two-dimensional electron gas (2DEG; density $4 \times 10^{11} \text{ cm}^{-2}$, mobility $3 \times 10^5 \text{ cm}^2/\text{Vs}$ at 2 K). By subsequent electron beam lithography and wet etching, QDs in the nanowire and constrictions in the 2DEG are defined simultaneously which ensures perfect alignment between QD and sensor (for details see Refs. 15 and 16). The parts of the

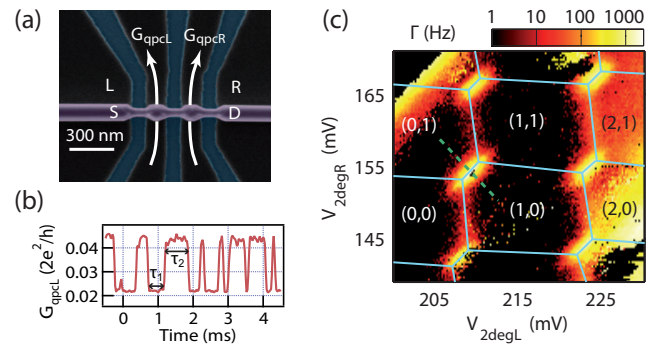


FIG. 1: (Color online) (a) SEM image of the device. A single etching step defines the DQD in the nanowire (horizontal) and constrictions in the 2DEG underneath. The white arrows indicate the direction of negative current through the point contacts. (b) Conductance G_{qpcL} of the left QPC measured time-resolved at a gate configuration where charge exchange between the dots is energetically allowed. The QPC conductance drops whenever an electron tunnels from the right into the left dot. (c) Charge stability diagram of the DQD obtained by evaluating the event rate $\Gamma = 1/(\tau_1 + \tau_2)$ in traces as in (b). The solid lines delineate regions of stable occupation numbers (n, m) of the DQD relative to the arbitrary reference $(0, 0)$. The subsequent measurements are carried out along the dashed line.

2DEG marked “L” and “R” serve as side gates to tune the QPC conductances. Similarly, the QPCs are used as gates to selectively tune the QD potentials by applying offset voltages $V_{2\text{degL}}$, $V_{2\text{degR}}$ to both source and drain. All measurements were done in a ^4He cryostat at $T = 2\text{ K}$.

The DQD is operated at zero source-drain voltage and is tuned to a regime with very opaque barriers where its charge dynamics is monitored with the QPC sensors. These are biased with source-drain voltages V_{qpcL} , V_{qpcR} , and their currents are measured with a bandwidth of 10 kHz. Figure 1(b) shows a typical time dependence of the left QPC’s conductance, which exhibits steps whenever a dot-charging event takes place. In measuring the event rate $\Gamma = 1/(\tau_1 + \tau_2)$ as a function of $V_{2\text{degL}}$ and $V_{2\text{degR}}$, we expect to reproduce the DQD charge stability diagram with nonzero Γ along the boundaries of the hexagonal regions of stable charge. In the corresponding graph in Fig. 1(c), which contains the data from the left QPC readout, we observe nearly vertical lines belonging to tunneling between the left QD and the source lead ($\sim 10\text{ Hz}$) and short, diagonal lines where interdot tunneling takes place ($\sim 1\text{ kHz}$). The horizontal charging lines of the right dot are only visible in the time-averaged signal (not shown), as the associated dot-drain transitions are too fast to be resolved in real time. The absolute occupation numbers of the two dots are not known, and hence the index pairs (n, m) assigned to the hexagons mark the excess electron numbers relative to the state labeled $(0, 0)$.

Apart from the features associated with the DQD, counts are detected in the $(2,0)$ and $(2,1)$ regions, as well as in the top left corner of the plot 1(c). We attribute these additional fluctuations to charge traps residing in the vicinity of the QPCs. Performing the measurements in the crossover region between charge states $(0,1)$ and $(1,0)$, we avoid disturbance by additional charge traps. We note that a change in QPC bias may trigger the activity of additional fluctuators, which however would leave clear signatures in the time-resolved current traces. In particular, additional amplitude- and time-scales characteristic for the dynamics of the charge trap would show up in the current traces on top of the DQD signal. In our experiments no such additional features have shown up.

In moving along the dashed line in Fig. 1(c), we continuously vary the energy difference $\delta = \mu_{\text{R}}^1 - \mu_{\text{L}}^1$ between the charge configurations $(1,0)$ and $(0,1)$, as illustrated in the level diagram in Fig. 2(a). The energies μ_{L}^2 and μ_{R}^2 required for doubly occupying the DQD are higher by the mutual charging energy $E_m \approx 0.8\text{ meV}$, which was determined by finite-bias spectroscopy. An electron in the lower-energy dot can tunnel to the higher-energy dot by absorbing an energy quantum $|\delta|$ from the environment. The DQD system therefore acts as a tunable and frequency-selective probe for electrical noise in its vicinity.^{11,7}

By applying a voltage $V_{\text{qpcL(R)}}$ across one of the QPCs,

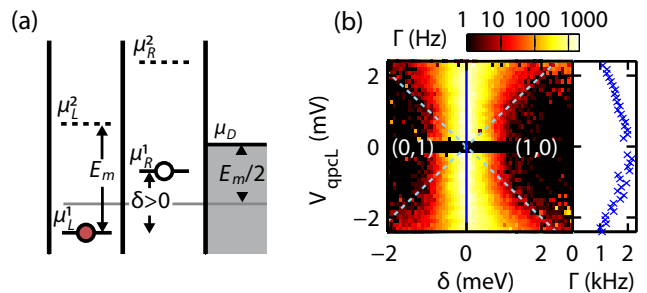


FIG. 2: (Color online) (a) Energy-level diagram of the DQD system and the drain lead. Upon adding a second electron to the DQD, the levels μ_{L}^1 , μ_{R}^1 shift by the mutual charging energy E_m to the new positions μ_{L}^2 , μ_{R}^2 . (b) Grayscale (colorscale) plot of the interdot tunneling rate Γ as a function of level detuning δ [dashed line in Fig. 1(c) with $(\mu_{\text{L}}^1 + \mu_{\text{R}}^1)/2 = \mu_{\text{D}} - E_m/2$] and source-drain voltage V_{qpcL} across the left QPC. Photons with energies bounded by $|eV_{\text{qpcL}}|$ are emitted by the QPC and can drive inelastic tunneling events which leads to a broadening of the main peak (dashed lines indicate the condition $\delta = \pm eV_{\text{qpcL}}$). The plot on the right is a cut through $\delta = 0\text{ meV}$ (solid line).

we generate broadband noise with a high-frequency cut-off at $eV_{\text{qpcL(R)}}/h$, meaning that the electrons passing through the QPC have an exponentially small probability to emit photons with energies higher than the bias energy.^{17,18,19,7} Due to the capacitive coupling, the generated photons can be absorbed by the DQD and drive inelastic transitions. In measuring the interdot tunneling rate Γ as a function of δ for increasing QPC bias, we therefore expect the equilibrium tunneling peak at $\delta = 0$ to become broadened due to photon absorption in a window $|\delta| < |eV_{\text{qpcL(R)}}|$. In Fig. 2(b), we plot the corresponding measurement for bias applied across the left QPC. A small region $|V_{\text{qpcL}}| < 0.15\text{ mV}$, where the signal-to-noise ratio of the counting signal is not sufficient, is excluded from the data.

A remarkable feature of the data in Fig. 2(b) is the fact that not only the peak *width* is influenced by the QPC, but also its *amplitude*. The maximum Γ at $V_{\text{qpcL}} = \pm 2\text{ mV}$ is smaller by a factor of 0.6 compared to the maximum at $V_{\text{qpcL}} \approx 0\text{ mV}$. Direct gating by the voltage V_{qpcL} can be excluded as the origin because of the magnitude of the effect, and second because of the symmetry in positive and negative V_{qpcL} . A similar reduction in the resonant current through a QD as a function of QPC bias, has been reported in Ref. 12. There, the effect could be explained by the excitation of an electron on the dot to a higher-energy state, from where it had the chance to tunnel back to the source lead.

We propose that in our measurements dot-lead processes are not relevant; this will be justified in more detail later in this paper. Instead, the reduction in Γ at zero δ is directly linked to its increase at non-zero δ via shift of spectral weight. For the discussion of this effect, we consider the QPC as a source of voltage noise, i.e., potential fluctuations $\hat{V}(t)$ across the central dot barrier

with a spectral density which we denote $S_V(\omega)$. Such fluctuations lead to inelastic tunneling through the central barrier, which is expressed in terms of the probability density for the dot to exchange energy quanta E with the source of the field,²⁰

$$P(E) = \frac{1}{2\pi\hbar} \int dt \exp [J(t) + iEt/\hbar]. \quad (1)$$

Here, the potential fluctuations are described in terms of the autocorrelation function $J(t) = \langle [\hat{\phi}(t) - \hat{\phi}(0)]\hat{\phi}(0) \rangle$ of the phase operators $\hat{\phi}(t) = \int_0^t dt' e^{\hat{V}(t')/\hbar}$. Equation (1) is valid for fields $\hat{V}(t)$ with typical frequencies much larger than the tunneling rate through the barrier, a regime in which $P(E)$ can be interpreted as the spectral density of the electronic state in either of the two dots. It is normalized to unity and determines the energy dependence of the unidirectional tunneling rates between the dots, namely, $\Gamma_{L\leftarrow R}(\delta) \equiv \Gamma_{LR}(\delta) \propto P(\delta)$ (right to left) and $\Gamma_{R\leftarrow L}(\delta) \propto P(-\delta)$ (left to right). Notably, the fact that $P(\delta)$ is not (necessarily) even in δ is due to the voltage $\hat{V}(t)$ being a quantum mechanical operator which does not commute with itself at different times, and hence $J(t) \neq J(-t)$ in Eq. (1). It is only within this (quantum) formalism that $P(\delta)$ can describe spontaneous emission of energy quanta into the modes of the field; if the voltage were classical, only stimulated absorption and emission would be possible and $P(\delta)$ would be even in δ .

We are interested in the inelastic tunneling processes caused by the biased QPC. Other inelastic processes, however, are not negligible but instead even dominate over the QPC-driven processes. In particular, emission and absorption of phonons²¹ within the InAs wire is known to be the most important mechanism for inelastic interdot tunneling. Here, we treat these processes as a background noise present at zero QPC voltage. We therefore split the voltage fluctuations \hat{V} , or rather their spectral density $S_V(\omega)$, into an *equilibrium* part $S_V^{(0)}(\omega)$, which includes thermal fluctuations in the nanowire as well as contributions from the QPC, and an *excess* part $S_V^{\text{ex}}(\omega; V_{\text{qpcL}})$, generated by the QPC at finite voltage V_{qpcL} . The equilibrium contribution $S_V^{(0)}$ then determines the line shape of the rates $\Gamma_{RL,LR}$ at zero QPC voltage, while the finite-bias noise shifts weight to higher/lower energies. Since the exponents $J(t) = J^{(0)}(t) + J^{\text{ex}}(t)$ for the equilibrium and the excess noise contributions are additive, it follows from Eq. (1) that their probability densities $P^{\text{ex}}(E; V_{\text{qpcL}})$ and $P^{(0)}(E)$ have to be convolved to obtain the total $P(E)$. Identifying $P(\delta; V_{\text{qpcL}}) \propto \Gamma_{LR}(\delta; V_{\text{qpcL}})$ and $P^{(0)}(\lambda) \propto \Gamma_{LR}(\lambda; 0)$ (and likewise for Γ_{RL}), we can relate the rates at finite and zero bias,

$$\Gamma_{LR}(\delta; V_{\text{qpcL}}) = \int d\lambda \Gamma_{LR}(\lambda; 0) P^{\text{ex}}(\delta - \lambda; V_{\text{qpcL}}). \quad (2)$$

To leading order in J^{ex} , the probability density

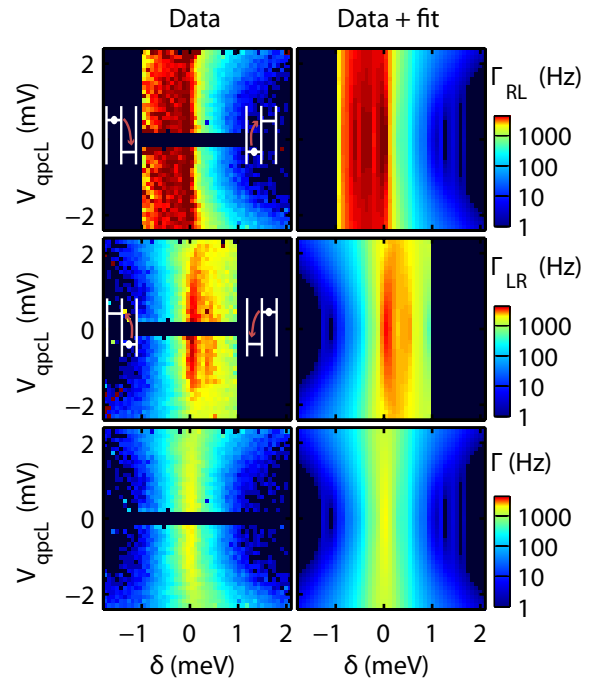


FIG. 3: (Color online) Left column: grayscale (colorscale) plots of the unidirectional tunneling rates $\Gamma_{LR,RL}$ and the total event rate Γ as functions of detuning δ and QPC bias V_{qpcL} . Some of the data (Γ_{RL} : $\delta < -1$ meV; Γ_{LR} : $\delta > 1$ meV) with large statistical errors have been removed. Right column: Theoretical V_{qpcL} -dependence of the data reconstructed by numerical convolution of the measured cuts at $V_{\text{qpcL}} = -460 \mu\text{V}$ (ideally $V_{\text{qpcL}} = 0 \mu\text{V}$) with the spectral density $P^{\text{ex}}(E; V_{\text{qpcL}})$, cf. Eq. (3).

$P^{\text{ex}}(E; V_{\text{qpcL}})$ can be expressed¹¹ through $S_V^{\text{ex}}(\omega; V_{\text{qpcL}})$,

$$P^{\text{ex}}(E; V_{\text{qpcL}}) = \left[1 - \frac{e^2}{\hbar^2} \int d\omega \frac{S_V^{\text{ex}}(\omega; V_{\text{qpcL}})}{\omega^2} \right] \delta(E) + \frac{e^2}{\hbar} \frac{S_V^{\text{ex}}(E/\hbar; V_{\text{qpcL}})}{E^2}. \quad (3)$$

We assume S_V^{ex} to be proportional to the current shot-noise S_I^{ex} of the QPC, which amounts to assuming a frequency-independent trans-impedance Z_{tr} relating the two. The symmetrized version of the shot-noise has been calculated by Khlus¹⁷ and by Lesovik,¹⁸ while the non-symmetrized expression has been found in Refs. 22 and 11. Depending on the specific detector design, it is the non-symmetrized noise which is usually measured in an experiment, either at positive frequencies only²² or at both positive and negative frequencies, as is the case in Refs. 11 and 23 as well as here. In the latter case, the asymmetry between positive and negative frequency results provides information on zero-point fluctuations (at sufficiently high frequencies as compared to the applied voltage and temperature). In the present situation, the excess noise is symmetric in frequency and hence we do

not get access to those fluctuations (cf. Ref. 23 for a situation where a non-symmetric excess noise is measured). The expression for the excess noise easily derives from the result in Ref. 11 or, since it is symmetric, from the original symmetrized results in Refs. 17 and 18,

$$S_I^{\text{ex}}(\omega; V_{\text{qpcL}}) = \frac{2e^2}{h} D(1-D) \left[-2\hbar\omega \coth\left(\frac{\hbar\omega}{2k_B T}\right) + (eV_{\text{qpcL}} + \hbar\omega) \coth\left(\frac{eV_{\text{qpcL}} + \hbar\omega}{2k_B T}\right) + (eV_{\text{qpcL}} - \hbar\omega) \coth\left(\frac{eV_{\text{qpcL}} - \hbar\omega}{2k_B T}\right) \right], \quad (4)$$

where $D = G_{\text{qpcL}}\hbar/(2e^2)$ is the transmission coefficient of the QPC. The noise spectrum (4) is even in ω , with a maximum at $\omega = 0$, and is characterized by a high-frequency cutoff $|\omega| < |eV_{\text{qpcL}}/\hbar|$ that is smeared by temperature.

Experimentally, we extract the rates $\Gamma_{\text{LR,RL}}$ from traces as that shown in Fig. 1(b) by averaging the time the signal spends in the low- or high-current state,² $\Gamma_{\text{RL}} \approx 1/\langle\tau_1\rangle$ and $\Gamma_{\text{LR}} \approx 1/\langle\tau_2\rangle$. In the left column of Fig. 3, we plot these rates as functions of V_{qpcL} and δ . [For clarity, we also include the plot of $\Gamma = \Gamma_{\text{LR}}\Gamma_{\text{RL}}/(\Gamma_{\text{LR}} + \Gamma_{\text{RL}})$ identical to that in Fig. 2(b).] Indeed they qualitatively exhibit the principal features expected from Eq. (3) combined with the spectrum (4), namely, the reduction in their maxima around $\delta = 0$ and their increase on the excitation side of the δ axis (that is, $\delta > 0$ for Γ_{RL} , and $\delta < 0$ for Γ_{LR}).

For the quantitative comparison between experiment and theory, we simulated the effect of the QPC by numerically performing the convolution of the energy density (3) with the measured rates at a QPC bias close to zero, according to Eq. (2). The only unknown parameter in this analysis is the trans-impedance Z_{tr} in $S_V^{\text{ex}}(\omega; V_{\text{qpcL}}) = |Z_{\text{tr}}|^2 S_I^{\text{ex}}(\omega; V_{\text{qpcL}})$ that was determined by minimizing the fitting error (weighted according to the inverse experimental uncertainty). Some care has to be taken concerning the coefficient D appearing in the noise spectrum (4). As seen in Fig. 1(b), the relative changes in G_{qpcL} caused by the hopping dot electron are large and the D coefficient relevant for the L→R processes (corresponding to the low-current state of the QPC signal, $D_{\text{L}} = 0.021$) is therefore significantly different from the one relevant for R→L processes ($D_{\text{R}} = 0.045$). The result of the analysis is given in the bottom row of Fig. 3 and shows a good agreement between theory and experiment. Both data sets, $\Gamma_{\text{LR}}(\delta; V_{\text{qpcL}})$ and $\Gamma_{\text{RL}}(\delta; V_{\text{qpcL}})$, are best approximated using a trans-impedance of $Z_{\text{tr}} = 5.4\text{ k}\Omega$. This value is roughly one order of magnitude larger than the corresponding figure given in Ref. 12, a fact which is well explained with the stronger capacitive coupling in the present case.

In order to rule out alternative explanations of the data, we shortly discuss how QPC-driven tunneling between right dot and lead may affect the measurement of $\Gamma_{\text{LR,RL}}$, and may account for the reduction in the tunneling rates near $\delta = 0\text{ meV}$. Namely, when allowing for

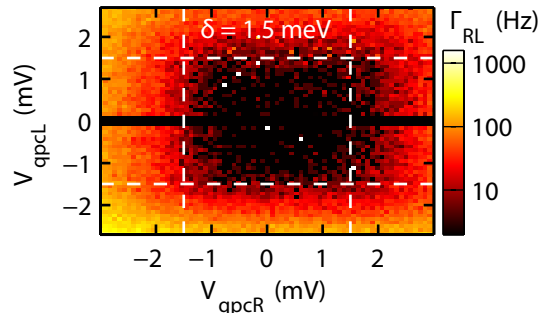


FIG. 4: (Color online) Photon-absorption rate Γ_{RL} as a function of the left and right QPC source-drain voltages measured at fixed detuning $\delta = 1.5\text{ meV}$ (dashed lines).

such dot-lead tunneling, the rate $\Gamma_{\text{LR}}(\delta \approx 0\text{ meV})$ would become smaller for increasing bias V_{qpcL} because an electron on the right dot may be excited into the lead (and tunnel back) instead of tunneling into the left dot. In the case of $\Gamma_{\text{RL}}(\delta \approx 0\text{ meV})$ instead, the possible mechanism would involve excitation *into* the dot: the QPC may overcome the mutual charging energy and excite an electron from the lead into the right dot, thus blocking tunneling from left to right dot [see also Fig. 2(a)].

However, such dot-lead processes take place predominantly as compositions of excitations to an intermediate state and subsequent elastic tunneling into the lead⁸ (or, in the other direction, excitation of the valence electron of the dot and subsequent tunneling from the lead into the unoccupied low-energy state). This is in contradiction to the fact that there is no indication of an onset in bias voltage in the data, which should be present at the energy of the excited state, if dot-lead processes were relevant. Instead, the changes in $\Gamma_{\text{RL,LR}}$ are smooth and gradual, and already significant at eV_{qpcL} values below the typical single-particle excitation energy of 0.8 meV in our sample. Furthermore, we stress that the PAT theory is able to quantify the behavior of the rates on and off peak with a *single* parameter, whereas in a model incorporating dot-lead processes these two are separate regimes.

For all measurements presented up to now, the right QPC's source-drain voltage was set to zero. Similar to the left QPC, it is tuned to a low conductance of approximately $0.08e^2/h$, and can be used as a noise source. This allows to test whether the perturbations created by the two QPCs have independent effects on the dot. To this end, we fix the detuning at a value of $\delta = 1.5\text{ meV}$ and measure Γ_{RL} (i.e., the photon-absorption rate) as a function of left and right QPC bias voltages. The result, shown in Fig. 4, is a plot with a characteristic, square structure with a region of zero absorption in the inner part. This confirms the picture described above in the sense that there is a well-defined energy threshold for one-photon processes ($|eV_{\text{qpcL}}|, |eV_{\text{qpcR}}| > |\delta|$), and that to first order the effects of the two QPCs add independently. Two-photon processes with pho-

tons arriving at the double dot originating from the two QPCs would result in an additional, possibly diamond-like structure due to the differing energy conservation condition $|eV_{\text{qpcL}}| + |eV_{\text{qpcR}}| \geq |\delta|$. A measurement of the kind shown in Fig. 4 provides a unique way of directly mapping the addition of energies of photons²⁴ emitted by different sources.

We have investigated the process of photon-assisted tunneling driven by QPC noise in an InAs based DQD. Due to the full tunability of the DQD, we could observe the expected suppression of tunneling for zero dot detun-

ing with increasing noise strength compensating for the increase in tunneling for nonzero detuning. Our data can be understood by treating the QPC as a high-frequency noise source. Finally, by measurements with two separate emitter QPCs we confirm that their effects add up independently.

The authors thank F. Portier, G. Lesovik, and S. Ludwig for fruitful discussion. Financial support from the Swiss National Science Foundation (Schweizerischer Nationalfonds) is gratefully acknowledged.

-
- * Electronic address: kuengb@phys.ethz.ch
- ¹ J. M. Elzerman, R. Hanson, L. H. W. van Beveren, B. Witkamp, L. M. K. Vandersypen, and L. P. Kouwenhoven, *Nature (London)* **430**, 431 (2004).
 - ² S. Gustavsson, R. Leturcq, B. Simovic, R. Schleser, T. Ihn, P. Studerus, K. Ensslin, D. C. Driscoll, and A. C. Gossard, *Phys. Rev. Lett.* **96**, 076605 (2006).
 - ³ T. Fujisawa, T. Hayashi, R. Tomita, and Y. Hirayama, *Science* **312**, 1634 (2006).
 - ⁴ J. Bylander, T. Duty, and P. Delsing, *Nature (London)* **434**, 361 (2005).
 - ⁵ S. Gustavsson, I. Shorubalko, R. Leturcq, S. Schön, and K. Ensslin, *Appl. Phys. Lett.* **92**, 152101 (2008).
 - ⁶ M. Field, C. G. Smith, M. Pepper, D. A. Ritchie, J. E. F. Frost, G. A. C. Jones, and D. G. Hasko, *Phys. Rev. Lett.* **70**, 1311 (1993).
 - ⁷ S. Gustavsson, M. Studer, R. Leturcq, T. Ihn, K. Ensslin, D. C. Driscoll, and A. C. Gossard, *Phys. Rev. Lett.* **99**, 206804 (2007).
 - ⁸ S. Gustavsson, I. Shorubalko, R. Leturcq, T. Ihn, K. Ensslin, and S. Schön, *Phys. Rev. B* **78**, 035324 (2008).
 - ⁹ V. S. Khrapai, S. Ludwig, J. P. Kotthaus, H. P. Tranitz, and W. Wegscheider, *Phys. Rev. Lett.* **97**, 176803 (2006).
 - ¹⁰ U. Gasser, S. Gustavsson, B. Küng, K. Ensslin, T. Ihn, D. C. Driscoll, and A. C. Gossard, *Phys. Rev. B* **79**, 035303 (2009).
 - ¹¹ R. Aguado and L. P. Kouwenhoven, *Phys. Rev. Lett.* **84**, 1986 (2000).
 - ¹² E. Onac, F. Balestro, L. H. Willems van Beveren, U. Hartmann, Y. V. Nazarov, and L. P. Kouwenhoven, *Phys. Rev. Lett.* **96**, 176601 (2006).
 - ¹³ L. M. K. Vandersypen, J. M. Elzerman, R. N. Schouten, L. H. Willems van Beveren, R. Hanson, and L. P. Kouwenhoven, *Appl. Phys. Lett.* **85**, 4394 (2004).
 - ¹⁴ R. Schleser, E. Ruh, T. Ihn, K. Ensslin, D. C. Driscoll, and A. C. Gossard, *Appl. Phys. Lett.* **85**, 2005 (2004).
 - ¹⁵ I. Shorubalko, R. Leturcq, A. Pfund, D. Tyndall, R. Krichcek, S. Schön, and K. Ensslin, *Nano Lett.* **8**, 382 (2008).
 - ¹⁶ T. Choi, I. Shorubalko, S. Gustavsson, S. Schön, and K. Ensslin, *New J. Phys.* **11**, 013005 (2009).
 - ¹⁷ V. A. Khlus, *Sov. Phys. JETP* **66**, 1243 (1987).
 - ¹⁸ G. B. Lesovik, *JETP Lett.* **49**, 592 (1989).
 - ¹⁹ E. Zakka-Bajjani, J. Ségala, F. Portier, P. Roche, D. C. Glattli, A. Cavanna, and Y. Jin, *Phys. Rev. Lett.* **99**, 236803 (2007).
 - ²⁰ M. H. Devoret, D. Esteve, H. Grabert, G.-L. Ingold, H. Pothier, and C. Urbina, *Phys. Rev. Lett.* **64**, 1824 (1990).
 - ²¹ T. Fujisawa, T. H. Oosterkamp, W. G. van der Wiel, B. W. Broer, R. Aguado, S. Tarucha, and L. P. Kouwenhoven, *Science* **282**, 932 (1998).
 - ²² G. B. Lesovik and R. Loosen, *JETP Lett.* **65**, 295 (1997).
 - ²³ P.-M. Billangeon, F. Pierre, R. Deblock, and H. Bouchiat, *J. Stat. Mech.* (2009), P01041.
 - ²⁴ J. Tobiska, J. Danon, I. Snyman, and Y. V. Nazarov, *Phys. Rev. Lett.* **96**, 096801 (2006).